

# Refractive index measurements of liquids from 0.5 to 2 $\mu\text{m}$ using Rayleigh interferometry

HAO-JUNG CHANG,<sup>1,4</sup> NATALIA MUNERA,<sup>1,4</sup> CESAR LOPEZ-ZELAYA,<sup>1,2</sup> DEBASMITA BANERJEE,<sup>1</sup> GUY BEADIE,<sup>3</sup> ERIC W. VAN STRYLAND,<sup>1</sup> AND DAVID J. HAGAN<sup>1,\*</sup>

<sup>1</sup>CREOL, The College of Optics and Photonics, University of Central Florida, Orlando, FL 32816, USA

<sup>2</sup>Air Force Research Laboratory, Munitions Directorate, Eglin AFB, FL 32542, USA

<sup>3</sup>Peak Nano Optics, LLC, Macedonia, OH 44056, USA

<sup>4</sup>These authors contributed equally to this work

\*[hagan@creol.ucf.edu](mailto:hagan@creol.ucf.edu)

**Abstract:** There is growing interest in the refractive index of liquids beyond the visible and into the short-wave infrared (SWIR) for applications such as the study of liquid-core fibers and supercontinuum generation. However, most of the data reported is in the visible. For liquids with a wide transmission window in the SWIR region, refractive index data are sparse. We present a Rayleigh interferometry-based refractometer to characterize the refractive index relative to standard materials at seven different wavelengths (543.5, 632.8, 780, 973, 1064, 1550, and 1970 nm) at a temperature of  $\sim 21.3 \pm 0.6$  °C. We also show Sellmeier fits using our results juxtaposed with previously published data. Our data extends previous work to the SWIR.

## 1. Introduction

The refractive index of liquids has been widely studied in the visible region. Nevertheless, in the SWIR region, there is a lack of data and the dispersion of the refractive index of most liquids is not known. The lack of both is especially true for hydrogen-free solvents, which can exhibit wide transmission windows in the SWIR [1, 2]. Some notable examples studied here include carbon tetrachloride, tetrachloroethylene, pentafluorobenzonitrile, bromotrichloromethane, and perfluorohexane. These solvents are good candidates for a variety of recent applications such as in liquid-core optical fibers [3–9], supercontinuum generation [7, 10], filamentation [11], nonlinear optics [12], and the design of optofluidic devices [13, 14].

Various techniques have been developed to measure the refractive index of liquids. One notable method is Abbe refractometry [15–17], where a liquid is positioned between two prisms, and the refractive index is calculated from Snell's law by measuring the angle at which total internal reflection at the liquid-prism interface occurs. Another technique is minimum deviation [18–22], which involves placing a liquid in a hollow prism and determining its refractive index by minimizing the angle between incident and deflected beams. In a similar method known as beam displacement [23–25], a liquid is contained in a cuvette, and a position-sensitive detector in the far field tracks the movement of the transmitted beam while the cuvette is rotated. With the ellipsometry technique [26,27], the real and imaginary part of the refractive index can be measured by measuring the polarization state change of light at various interfaces, such as air-liquid, prism-liquid, or liquid-solid interfaces. A different approach involves using the Kramers-Kronig relations to calculate the refractive index of a liquid from its absorption spectrum [28]. Finally, there are interferometric techniques, such as Michelson interferometry [29–31] using white light, interference between reflected and transmitted beams from the liquid [32], and interference between a beam passing through the liquid and another passing through a material of known index [33–36].

We report a technique for measuring the refractive index of liquids by measuring the relative phase between two beams as a function of change in optical path length using a Rayleigh interferometer [37]. Here, the interference is between a beam passing through a sample liquid

47 with unknown refractive index and a beam passing through a reference material with a known  
 48 refractive index, both beams originating from the same source. We found this technique to be  
 49 simple to setup, accurate (depending on the choice of reference material and curve fitting), and  
 50 effective in cases of high loss due to absorption of the sample being measured. We performed  
 51 this experiment at seven wavelengths (543.5, 632.8, 780, 973, 1064, 1550, and 1970 nm) at a  
 52 temperature of  $\sim 21.3 \pm 0.6$  °C. The dispersion is reported in the form of Sellmeier equations,  
 53 which are applicable from 543.5 nm to 1970 nm. We include both our experimental results and  
 54 values reported in the literature spanning the range from 400 nm to 2000 nm.

## 55 2. Experiment

56 The Rayleigh interferometer [37] used in this work is shown in Fig. 1(a). A laser source passes  
 57 through a half-wave plate (HWP) located between a pair of polarizers (P) to control the power  
 58 and polarization. The beam then passes through a spatial filter (SF) and is collimated by the first  
 59 lens ( $L_b$ ) to form a Gaussian beam (the spatial profile of the 1970 nm case was good enough to  
 60 not need the spatial filter). This Gaussian beam passes through an opaque plate with two 0.5 mm  
 61 holes with a center-to-center distance of  $h \approx 1.3$  mm to produce two beamlets: the reference  
 62 beam and the sample beam. For both 1550 nm and 1970 nm, a plate with 0.8 mm holes and  
 63  $h \approx 2.8$  mm is used. The beamlets are incident on a Starna 63-Q-10 Spectrosil quartz cuvette  
 64 with two internal chambers of  $10 \pm 0.01$  mm pathlength. One beamlet goes through the sample  
 65 liquid while the other goes through the reference liquid. In the case of using fused silica as the  
 66 reference, the Starna 29F-Q-10 cuvette has a single  $10 \pm 0.01$  mm pathlength liquid chamber and  
 67 the other side is fused silica; essentially mimicking a chamber filled with solid glass. The two  
 68 spatially and temporally coherent beamlets are then weakly focused by a second lens ( $L_f$ ) of focal  
 69 length  $f = 1000$  mm for 1064 nm and shorter, and  $f = 750$  mm for both 1550 nm and 1970 nm,  
 70 to create interference fringes. These fringes are measured on one of two cameras, or a detector,  
 71 depending on the wavelength as described below.

72 The interference pattern was recorded while the cuvette was rotated to measure the phase  
 73 difference between the reference and the sample. Since the refractive index of the reference and  
 74 the sample liquid are different, the two beamlets travel different optical paths as shown in Fig.  
 75 1(b). Hence, the relative phase difference between the beamlets can be written as:

$$\Delta\phi(\theta_{in}) = \frac{2\pi L}{\lambda_0} \left[ \sqrt{n_{sam}^2 - \sin^2 \theta_{in}} - \sqrt{n_{ref}^2 - \sin^2 \theta_{in}} \right] - \Delta\phi_0, \quad (1)$$

76 where  $\theta_{in}$  is the angle of incidence,  $\lambda_0$  is the vacuum wavelength,  $n_{sam}$  and  $n_{ref}$  are the sample  
 77 and reference relative refractive indices, respectively, and  $\Delta\phi_0 = \frac{2\pi L}{\lambda_0} [n_{sam} - n_{ref}]$  is included to  
 78 ensure that  $\Delta\phi(0^\circ) = 0$ . The relative refractive index is defined as a material's absolute refractive  
 79 index divided by the refractive index of the surrounding air, which is a measure of the material's  
 80 refractive power in air. We follow the standard practice used in optical glass catalogs and provide  
 81 dispersion data in the form of relative refractive index values. Unless otherwise stated, all results  
 82 and tabulated coefficients refer to the presentation of relative refractive index values as a function  
 83 of vacuum wavelengths.

84 As the cuvette is rotated, the beamlets undergo different displacements due to refraction. These  
 85 vertical displacements,  $\delta Y_{sam}(\theta_{in})$  and  $\delta Y_{ref}(\theta_{in})$ , result in an additional pathlength,  $\delta P(\theta_{in})$ ,  
 86 as shown in Fig.1(b) – the additional pathlength,  $\delta P(\theta_{in})$ , is accounted for in Eq. 1. The  
 87 expressions for  $\delta Y_{sam}(\theta_{in})$  and  $\delta Y_{ref}(\theta_{in})$  were derived in [23] and are given by:  $\delta Y_{sam}(\theta_{in}) =$   
 88  $\left[ 2L_g \left( 1 - \frac{\cos \theta_{in}}{\sqrt{n_g^2 - \sin^2 \theta_{in}}} \right) + L \left( 1 - \frac{\cos \theta_{in}}{\sqrt{n_{sam}^2 - \sin^2 \theta_{in}}} \right) \right] \sin \theta_{in}$ , where  $L_g = 1.25$  mm is the thickness of  
 89 the cuvette walls, and  $n_g$  is the refractive index of Spectrosil quartz at a specific wavelength; a  
 90 similar expression where  $n_{ref}$  is used instead corresponds to  $\delta Y_{ref}(\theta_{in})$ .

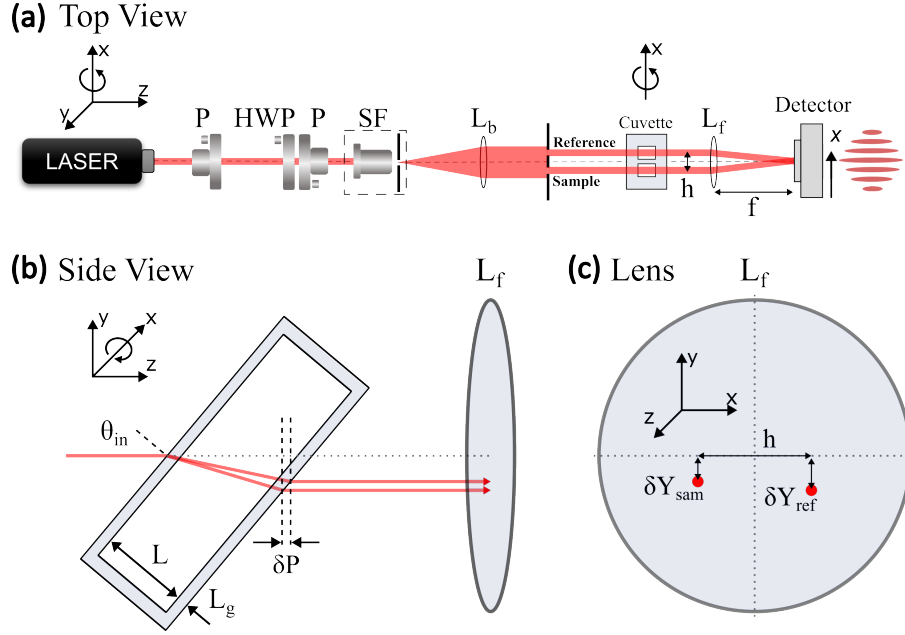


Fig. 1. (a) Top view of the optical setup. (b) Side view showing how rotating the cuvette about the  $x$ -axis changes the incident angle,  $\theta_{in}$ . The beamlets refract at different angles and experience different optical paths due to the refractive indices of the sample,  $n_{sam}$ , and reference,  $n_{ref}$ . (c) Consequently, the beamlets become vertically misaligned on the second lens,  $L_f$ , by  $\delta Y_{sam}$  and  $\delta Y_{ref}$ .

91 In Fig. 1(b) and (c), the beam separations are greatly exaggerated to show the pathlength  
 92 differences. In actuality, for a maximum incident angle,  $\theta_{in} = 20^\circ$ ,  $n_{sam} > n_{ref}$  and  $n_{sam} -$   
 93  $n_{ref} \leq 0.1$ , the maximum change in the angle between the two beamlets within the cuvette  
 94 is  $\sim 1^\circ$ . Consequently, the difference in the vertical displacement of the two beamlets is  
 95  $\Delta Y(20^\circ) = \delta Y_{sam}(20^\circ) - \delta Y_{ref}(20^\circ) < 200 \mu\text{m}$ , as shown greatly exaggerated in Fig. 1(b) and  
 96 (c). The difference in the vertical displacement can lead to a slight  $xy$ -plane tilt of the fringes by  
 97 an angle  $\theta_{tilt} = \tan^{-1}(\Delta Y(20^\circ)/h)$ . This causes the spacing of the fringes to be slightly modified;  
 98 however, along the  $x$  direction, which is what is measured, the observed spacing is unchanged.  
 99 Additionally, for the lens effective  $f\# = h/f$  used in this work,  $\sim f/769$  for the visible (up to  
 100 1064 nm) and  $\sim f/268$  for the SWIR (1550 nm and 1970 nm), we can safely ignore aberrations.

101 The phase difference,  $\Delta\phi$ , changes with incident angle, causing the interference fringes to  
 102 move. To verify this, we used identical index matching liquids on the cuvette, which caused  
 103 the interference pattern to stay constant in response to the cuvette rotation. This proved to us  
 104 that the relative phase was unchanged. Fig. 2 shows the interferogram between a cyclohexane  
 105 sample (which is unknown in our case) and Fused Silica Matching Liquid Code 50350 (see Data  
 106 File 1) as the known reference. Fig. 2(a) shows the cross-section of the interference fringes as a  
 107 function of position on the camera for several different incident angles. As shown in the figure,  
 108 the interference maxima move as the cuvette is rotated. Fig. 2(b) shows the positions of the  
 109 maxima (red markers) as a function of incident angle. An additional step requires converting the  
 110 experimental data from pixels (or detector scans) to phase. The unknown refractive index of  
 111 the sample liquid,  $n_{sam}$ , is then obtained by fitting Eq. 1 (solid black lines) to the experimental  
 112 data, where the adjustable parameters are  $n_{sam}$  and the distance between consecutive interference  
 113 maxima converted from pixels (or detector scans) to phase.

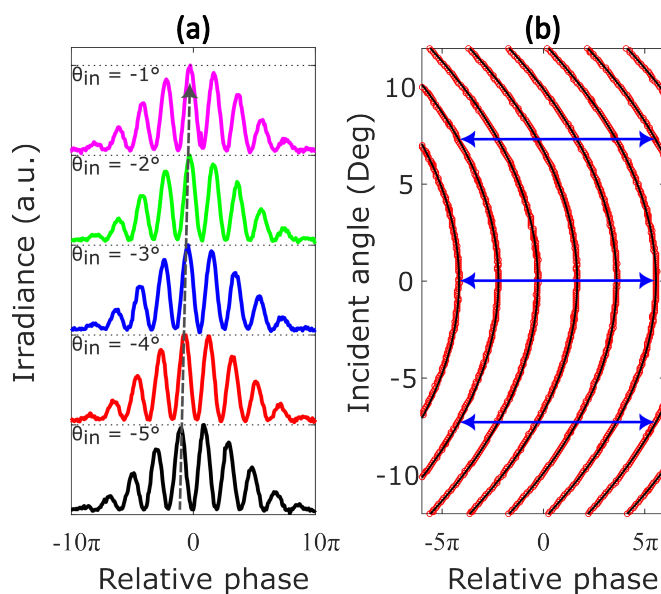


Fig. 2. (a) Cross-section of the interference fringes at five different incident angles for cyclohexane using fused silica index matching liquid as a reference at 543.5 nm. Gray dashed arrow represents fringe displacement. (b) Interference maxima plotted vs. incident angle from camera image (red markers) along with fits to Eq. 1 (solid black lines). Blue horizontal arrows of equal length represent a  $10\pi$  relative phase.

114 Seven laser sources were used: two helium-neon lasers with central wavelengths at 543.5 nm  
 115 (Melles Griot, 05-LGR-025-S) and 632.8 nm (Melles Griot, 05-LHP-171), two diode lasers with  
 116 central wavelengths at 780 nm and 973 nm (the wavelength was measured with an Ocean Optics  
 117 spectrometer), a microchip laser (Teem Photonics, MLC-0240DR1) at 1064 nm, a laser diode  
 118 module (Thorlabs, LDM1550) at 1550 nm and a thulium fiber laser (AdValue, AP-QS-MOD) at  
 119 1970 nm. The reference materials are the 29F-Q-10 cuvette wall (Spectrosil quartz from Heraeus)  
 120 and refractive index liquids from Cargille labs loaded on the side channel of the 63-Q-10 cuvette.  
 121 Cargille labs provided the refractive indices of the reference liquids relative to vacuum. To  
 122 convert these to values relative to air, we multiplied them by  $1/n_{\text{air}}$ . In contrast, the refractive  
 123 indices for the Spectrosil quartz reference were already given relative to air by Heraeus. For more  
 124 information on what reference material was used for each liquid at each wavelength, see Data  
 125 File 1. The detectors are a silicon beam profiler (Coherent, LASERCAM HR) for the shortest  
 126 five wavelengths, an InGaAs camera (Sensors Unlimited, SU640CSX) for 1550 nm, and a 20  
 127  $\mu\text{m}$  pinhole attached to a PbSe detector (Thorlabs, PDA20H) for 1970 nm. The silicon beam  
 128 profiler was used to generate the full fringe trajectory pattern shown in Fig. 2(b). This pattern  
 129 was generated through repeated scans at various incident angles, a process that only required  
 130 a few minutes. Similarly, employing the InGaAs camera at 1550 nm to generate equivalent  
 131 patterns also took only a few minutes. In contrast, scans with the PbSe detector at 1970 nm  
 132 took  $\sim 12$  hours. For instance, when examining trichloroacetonitrile at 1970 nm, the interference  
 133 fringes were scanned across 161 detector positions for each of the 151 incident angles. For the  
 134 angular rotations, a Newport universal motion controller driver model ESP300 was used to rotate  
 135 a Micro-Controle Spectra-Physics rotation stage. The temperature is measured by an external  
 136 thermometer (Xsensor). All measurements are done at  $\sim 21.3 \pm 0.6$  °C. All the solvents are  
 137 commercially available as referenced in Tables 1–5, and used without further purification.

### 138 3. Results

139 The experimental results are presented in Tables 1–5 along with literature data. The first column  
140 lists the sample liquids being characterized, their chemical formula, the vendors we obtained  
141 them from, and the average temperature at which the measurements were done. In the third  
142 column, parentheses indicate the total uncertainty ( $\pm$ ) in the 4th decimal place, while the fourth  
143 column's parentheses denote both the measurement temperature and the measurement uncertainty  
144 ( $\pm$ ) in the 4th decimal place, respectively. A star (\*) in the literature column indicates that the  
145 value is calculated from the dispersion function reported in the corresponding literature. Double  
146 stars (\*\*) in Ref. [28] indicate values calculated from Kramers-Kronig relations. The reference  
147 refractive index for each sample was typically chosen to yield an index difference,  $|n_{sam} - n_{ref}|$ ,  
148 between  $\sim 0.01$  and  $0.1$  to accurately fit Eq. 1 to the experimental data, such as in Fig. 2(b).  
149 Data File 1 contains the % transmittance spectrum for each sample measured with a Cary 5000  
150 spectrophotometer from 400 to 2000 nm. The transmittance spectrum for each sample includes  
151 the reflection loss from the 10 mm pathlength Spectrosil quartz cuvette. The absorption of the  
152 cuvette in this wavelength region is negligible. Data File 1 also includes the reference refractive  
153 index liquids used at each wavelengths.

Table 1. Relative refractive index of benzene derivatives in this work and literature

Liquid and Temp.	Wavelength (nm)	This work	Literature
Benzene C <sub>6</sub> H <sub>6</sub> Sigma-Aldrich T = 21.5 ± 0.4 °C	543.5	1.5037(5)	1.4999(27) [38], 1.5055(20) [33], 1.5056(20) [39]*,
	632.8	1.4964(5)	1.4925(27) [38]*, 1.495137(25) [36]*, 1.497866(20) [33]* 1.4980(20) [39]
	780	1.4888(2)	1.4859(27) [38], 1.4908(20) [39]
	973	1.4843(10)	1.4815(27) [38], 1.4857(20) [39]
	1064	1.4842(10)	1.4802(27) [38], 1.4814(25,1) [25]*, 1.4808(25,5) [25]*, 1.4841(20) [39]
	1550	1.4797(3)	1.4769(27) [38]*, 1.4789(25,3) [17], 1.4767(27) [28]*, 1.4777(27) [28]**, 1.4799(20) [39]
1970	1.4780(6)	1.4774(27) [28]**, 1.4784(20) [39]	
Toluene C <sub>6</sub> H <sub>5</sub> CH <sub>3</sub> ACROS T = 21.9 ± 0.8 °C	543.5	1.4993(5)	1.4961(27) [38], 1.5009(20) [16], 1.4979(20) [34], 1.5009(20) [39], 1.4996(22) [40]
	632.8	1.4914(6)	1.4890(27) [38]*, 1.4936(20) [16], 1.491218(25) [36]*, 1.495612(20) [34]*, 1.4936(20) [39], 1.4940(22) [40]
	780	1.4850(2)	1.4824(27) [38], 1.4870(20) [16], 1.4869(20) [39]
	973	1.4805(10)	1.4781(27) [38], 1.4825(20) [16], 1.4824(20) [39]
	1064	1.4800(10)	1.4769(27) [38], 1.4812(20) [16], 1.4784(25,1) [25]*, 1.4777(25,3) [25]*, 1.4811(20) [39]
	1550	1.4768(4)	1.4737(27) [38]*, 1.4778(20) [16], 1.4760(25,2) [17], 1.4735(27) [28]*, 1.4741(27) [28]**, 1.4777(20) [39]
1970	1.4753(4)	1.4744(27) [28]**, 1.4764(20) [39]	
P-Xylene C <sub>6</sub> H <sub>4</sub> (CH <sub>3</sub> ) <sub>2</sub> Sigma-Aldrich T = 21.8 ± 0.5 °C	543.5	1.4976(2)	
	632.8	1.4915(5)	
	780	1.4867(4)	
	973	1.4786(10)	
	1064	1.4800(10)	
1550	1.4759(3)	1.4753(25,1) [17]	
1970	1.4751(4)		
Pyridine C <sub>6</sub> H <sub>5</sub> N Sigma-Aldrich T = 21.7 ± 0.5 °C	543.5	1.5115(6)	
	632.8	1.5038(6)	
	780	1.4978(3)	
	973	1.4938(10)	
	1064	1.4923(10)	
1550	1.4880(3)	1.4851(27) [28]*, 1.4857(27) [28]**	
1970	1.4864(7)	1.5212(27) [28]**	
Nitrobenzene C <sub>6</sub> H <sub>5</sub> NO <sub>2</sub> Sigma-Aldrich T = 21.9 ± 0.8 °C	543.5	1.5567(6)	
	632.8	1.5462(7)	
	780	1.5353(5)	
	973	-	
	1064	1.5264(10)	1.5262(25,2) [25]*
1550	1.5223(5)	1.4125(25) [41]	
1970	1.5199(7)	1.5212(27) [28]**	

Table 2. Relative refractive index of haloalkanes in this work and literature

Liquid and Temp.	Wavelength(nm)	This work	Literature
Dichloromethane CH <sub>2</sub> Cl <sub>2</sub> Merck KGaA T = 21.6 ± 0.5 °C	543.5	1.4258(5)	
	632.8	1.4217(3)	
	780	1.4180(4)	
	973	-	
	1064	1.4150(10)	1.4120(6) [25]*
	1550	1.4133(2)	1.4124(25,2) [17], 1.4125(25) [41]
	1970	1.4126(4)	1.4121(25) [41]
Chloroform CHCl <sub>3</sub> Sigma-Aldrich T = 21.6 ± 0.8 °C	543.5	1.4472(2)	1.4464(20) [16], 1.4520(20) [34], 1.4485(20) [39]
	632.8	1.4436(5)	1.3323(20) [16], 1.441415(20) [34]*, 1.4443(20) [39]
	780	1.4380(4)	1.4385(20) [16], 1.4401(20) [39]
	973	1.4370(10)	1.4361(20) [16], 1.4371(20) [39]
	1064	1.4347(10)	1.4354(20) [16], 1.4331(25,4) [25]*, 1.4362(20) [39]
	1550	1.4332(10)	1.4334(20) [16], 1.4321(25,1) [17], 1.4337(20) [39]
	1970	1.4315(3)	1.4326(20) [39]
Carbon tetrachloride CCl <sub>4</sub> Sigma-Aldrich T = 22.0 ± 0.9 °C	543.5	1.4599(4)	1.4593(27) [38], 1.4621(20) [16]
	632.8	1.4566(4)	1.4551(27) [38]*, 1.4579(20) [16], 1.455852(25) [36]*
	780	1.4522(5)	1.4513(27) [38], 1.4539(20) [16]
	973	1.4510(10)	1.4488(27) [38], 1.4521(20) [16]
	1064	1.4498(10)	1.4481(27, 1) [38], 1.4504(20) [16], 1.4477(25,2) [25]*, 1.4557(25) [42]
	1550	1.4468(3)	1.4464(27) [38]*, 1.4483(20) [16], 1.4530(25) [42]
	1970	1.4457(2)	1.4530(25) [42]

Table 3. Relative refractive index of alcohols in this work and literature

Liquid and Temp.	Wavelength(nm)	This work	Literature
Methanol CH <sub>3</sub> OH ACROS T = 21.5 ± 0.3 °C	543.5	1.3292(4)	1.3284(27) [38], 1.3376(20) [33], 1.3295(22) [40]
	632.8	1.3270(5)	1.3259(27) [38]*, 1.326343(20) [33]*, 1.3270(22) [40]
	780	1.3224(5)	1.3234(27) [38]
	973	1.3210(10)	1.3215(27) [38]
	1064	1.3190(10)	1.3207(27) [38], 1.3198(25,3) [25]*
	1550	-	1.3172(27) [38]*, 1.3174(25,1) [17], 1.4201(26) [28]*, 1.3115(26) [28]**
	1970	1.3164(8)	1.3074(26) [28]**
Ethanol C <sub>2</sub> H <sub>5</sub> OH Sigma-Aldrich T = 21.6 ± 0.6 °C	543.5	1.3627(3)	1.3631(20) [16], 1.3626(22) [40]
	632.8	1.3604(3)	1.3603(20) [16], 1.358853(25) [36]*, 1.3593(22) [40]
	780	1.3580(6)	1.3575(20) [16]
	973	1.3543(10)	1.3554(20) [16]
	1064	1.3548(10)	1.3547(20) [16]
	1550	1.3523(10)	1.3520(20) [16], 1.3503(25,3) [17], 1.3495(26) [28]*, 1.3474(26) [28]**
	1970	1.3482(6)	1.3447(26) [28]**
1-propanol C <sub>3</sub> H <sub>8</sub> O Sigma-Aldrich T = 21.7 ± 0.7 °C	543.5	1.3863(3)	1.3846(27) [38]
	632.8	1.3828(4)	1.3941(27) [38]*, 1.397105(20) [33]*
	780	1.3810(5)	1.3913(27) [38]
	973	1.3783(10)	1.3890(27) [38]
	1064	1.3783(10)	1.3883(27) [38]
	1550	1.3751(10)	1.3858(27) [38]*
	1970	1.3725(4)	
1-butanol C <sub>4</sub> H <sub>10</sub> O Sigma-Aldrich T = 21.6 ± 0.6 °C	543.5	1.3999(2)	1.3970(27) [38]
	632.8	1.3978(2)	1.3941(27) [38]*, 1.397105(20) [33]*
	780	1.3950(4)	1.3913(27) [38]
	973	1.3922(10)	1.3890(27) [38]
	1064	1.3916(10)	1.3883(27) [38]
	1550	1.3890(10)	1.3858(27) [38]*
	1970	1.3868(6)	
1-octanol C <sub>8</sub> H <sub>18</sub> O Sigma-Aldrich T = 21.7 ± 0.6 °C	543.5	1.4305(2)	
	632.8	1.4273(2)	
	780	1.4235(4)	
	973	1.4226(10)	
	1064	1.4210(10)	
	1550	1.4190(10)	
	1970	1.4163(2)	



Table 4. Relative refractive index of SWIR transparent solvents

Liquid and Temp.	Wavelength(nm)	This work	Literature
Carbon disulfide CS <sub>2</sub> Sigma-Aldrich T = 21.7 ± 0.8 °C	543.5	1.6319(9)	1.6373(20) [9], 1.6361(20) [16], 1.6367(20) [39]
	632.8	1.6177(10)	1.6213(20) [9], 1.6211(20) [16], 1.617672(25) [36]*, 1.623977(20) [34]*, 1.6212(20) [39]
	780	1.6019(11)	1.6066(20) [9], 1.6072(20) [16], 1.6069(20) [39]
	973	-	1.5968(20) [9], 1.5981(20) [16], 1.5974(20) [39]
	1064	1.5950(10)	1.5939(20) [9], 1.5955(20) [16], 1.5910(25,3) [25]*, 1.5946(20) [39]
	1550	1.5834(7)	1.5857(20) [9], 1.5885(20) [16], 1.5872(20) [39]
Pentafluorobenzonitrile C <sub>6</sub> F <sub>5</sub> CN Sigma-Aldrich T = 21.6 ± 0.5 °C	1970	1.5802(10)	1.5812(20) [9], 1.5843(20) [39]
	543.5	1.4453(5)	
	632.8	1.4381(2)	
	780	1.4332(3)	
	973	1.4295(10)	
	1064	1.4240(10)	1.4254(25,4) [25]*
Bromotrichloromethane BrCCl <sub>3</sub> Sigma-Aldrich T = 21.6 ± 0.5	1550	1.4241(4)	
	1970	1.4213(4)	
	543.5	1.5080(6)	
	632.8	1.5016(5)	
	780	1.4958(2)	
	973	-	
Perfluorohexane C <sub>6</sub> F <sub>14</sub> Alfa Aesar T = 21.5 ± 0.3	1064	1.4932(10)	
	1550	1.4895(3)	
	1970	1.4881(6)	
	543.5	1.2524(4)	
	632.8	1.2509(4)	
	780	1.2495(6)	
Tetrachloroethylene C <sub>2</sub> Cl <sub>4</sub> Sigma-Aldrich T = 21.7 ± 0.6 °C	973	1.2480(10)	
	1064	1.2480(10)	
	1550	1.2475(10)	
	1970	1.2462(13)	
	543.5	1.5068(6)	
	632.8	1.5015(3)	
Trichloroacetonitrile C <sub>2</sub> Cl <sub>3</sub> N Sigma-Aldrich T = 21.5 ± 0.5 °C	780	1.4955(3)	
	973	1.4917(10)	
	1064	1.4907(10)	
	1550	1.4879(4)	
	1970	1.4864(5)	
	543.5	1.4382(4)	
Trifluoroacetic anhydride C <sub>4</sub> F <sub>6</sub> O <sub>3</sub> Sigma-Aldrich T = 21.1 ± 0.7 °C	632.8	1.4348(6)	
	780	1.4318(6)	
	973	-	
	1064	1.4280(10)	
	1550	1.4258(9)	
	1970	1.4265(8)	
Trifluoroacetic anhydride C <sub>4</sub> F <sub>6</sub> O <sub>3</sub> Sigma-Aldrich T = 21.1 ± 0.7 °C	543.5	1.2708(5)	
	632.8	1.2685(3)	
	780	1.2661(5)	
	973	-	
	1064	1.2645(10)	
	1550	1.2641(9)	
1970	1.2628(11)		

Table 5. Relative refractive index of other common solvents

Liquid and Temp.	Wavelength(nm)	This work	Literature
Acetone ( $C_3H_6O$ ) Sigma-Aldrich $T = 21.5 \pm 0.2$ °C	543.5	1.3590(5)	
	632.8	1.3568(4)	
	780	1.3525(5)	
	973	1.3520(10)	
	1064	1.3490(10)	1.3487(25,4) [25]*
	1550	1.3487(10)	1.3483(25,2) [17]
Acetonitrile ( $C_2H_3N$ ) Sigma-Aldrich $T = 21.4 \pm 0.3$ °C	543.5	1.3440(3)	1.3418(27) [38], 1.3438(22) [40]
	632.8	1.3416(6)	1.3393(27) [38]*, 1.3408(22) [40]
	780	1.3395(5)	1.3373(27) [38]
	973	1.3365(10)	1.3361(27) [38]
	1064	1.3357(10)	1.3357(27) [38], 1.3354(25,3) [25]*
	1550	1.3358(10)	1.3345(27) [38]*, 1.3335(26) [28]*, 1.3337(26) [28]**, 1.3348(25,2) [17]
1970	1.3339(7)	1.3335(26) [28]**	
Hexane $C_6H_{14}$ Sigma-Aldrich $T = 21.5 \pm 0.5$ °C	543.5	1.3770(4)	1.3776(22) [40]
	632.8	1.3736(3)	1.3743(22) [40]
	780	1.3712(5)	
	973	1.3688(10)	
	1064	1.3698(10)	
	1550	1.3670(10)	
1970	1.3668(3)		
Cyclohexane $C_6H_{12}$ ACROS $T = 21.5 \pm 0.6$ °C	543.5	1.4268(3)	1.4273(22) [40]
	632.8	1.4242(2)	1.4238(22) [40]
	780	1.4215(4)	
	973	1.4185(10)	
	1064	1.4180(10)	1.4158(25,4) [25]*
	1550	1.4158(3)	1.4147(25,11) [17]
1970	1.4147(4)		
Tetrahydrofuran $C_4H_8O$ ACROS $T = 21.6 \pm 0.7$ °C	543.5	1.4084(2)	
	632.8	1.4053(2)	
	780	1.4025(3)	
	973	1.4008(10)	
	1064	1.4000(10)	1.3974(25,1) [25]*
	1550	1.3983(10)	1.3969(25,3) [17]
1970	1.3961(4)		
1,4-Dioxane $C_4H_8O_2$ Sigma-Aldrich $T = 21.6 \pm 0.5$ °C	543.5	1.4241(3)	1.4219(27) [38]
	632.8	1.4197(5)	1.4190(27) [38]*
	780	1.4179(3)	1.4165(27) [38]
	973	1.4148(10)	1.4148(27) [38]
	1064	1.4150(10)	1.4143(27) [38], 1.4119(25,2) [25]*
	1550	1.4123(10)	1.4124(27) [38]*, 1.4127(25, 5) [17]
1970	1.4108(4)		

154 The primary contributors to the uncertainty in the measured refractive indices include the  
 155 uncertainty in the index of the reference material, as provided by the manufacturer (see Data  
 156 File 1), and the fitting uncertainties. To determine the fitting error, we identified the value  
 157 of  $n_{sam}$  and the distance between consecutive interference maxima converted from pixels (or  
 158 detector scans) to phase that best fits Eq. 1 to the experimental data (e.g., red markers in Fig.  
 159 2(b)). We then adjusted  $n_{sam}$  by an offset  $\pm\Delta$  that fit the experimental data adequately. The  
 160 range between the highest and lowest refractive indices that still produced adequate fits of the  
 161 data determines  $\Delta n_{sam}$ , i.e., the fitting uncertainties. For most liquids, the fitting error was  
 162  $\Delta n_{sam} \lesssim 3 \cdot 10^{-4}$ . The total uncertainties including the reference etc. are in Tables 1–5 but in  
 163 general are  $\lesssim 10 \cdot 10^{-4}$ , while perfluorohexane and trifluoroacetic anhydride, the liquids with  
 164 the lowest refractive indices, exhibited maximum fitting uncertainties in the order of  $\sim 13 \cdot 10^{-4}$ .  
 165 Ultimately, the total uncertainties can be reduced, i.e., the technique’s accuracy can be increased,  
 166 by choosing well-calibrated reference materials with lower uncertainty in their refractive index  
 167 and with improved curve-fitting algorithms.

168 We also considered uncertainties due to temperature, geometrical tolerances of the cuvette,  
 169 and laser wavelength. However, these uncertainties were smaller than the primary contributors  
 170 discussed above. Temperatures in the laboratory fluctuated by  $\sim 1\%$  resulting in uncertainties  
 171 beyond the resolution limit set forth by the experiment. The cuvette pathlength is known to an  
 172 accuracy of 0.1% (from the manufacturer, Starna), however knowing the accuracy is redundant  
 173 due to both the sample and reference liquids being in the same cuvette. For the contribution  
 174 of the wavelength uncertainty to remain below the  $2 \cdot 10^{-4}$  threshold, which is the lowest total  
 175 uncertainty reported in Tables 1–5, the maximum tolerable uncertainty for the wavelengths we  
 176 used (543.5, 632.8, 780, 973, 1064, 1550, 1970 nm) is  $\pm (0.5, 0.8, 1.6, 3.0, 3.8, 8.4, 9.2 \text{ nm})$ ,  
 177 respectively. Although the incident angle is a variable in Eq. 1, angle readout does not give an  
 178 uncertainty – it only needs to be consistent, i.e., the separation of each interference fringe needs  
 179 to be consistent. We do not need to know the absolute angle since  $\Delta\phi(0^\circ)$  is the origin of the Eq.  
 180 1 centered at  $0^\circ$ . However, we do need to know the relative angle change

181 Despite the high loss due to absorption of some liquids at specific wavelengths, such as 1550  
 182 nm for the alcohols, the refractive index could still be measured with a fringe peak-to-minimum  
 183 contrast as low as 0.7% – corresponding to ethanol. Ideally, from the equation of interference  
 184 of two beams (assuming monochromatic plane-waves), we expect a  $\sim 20\%$  fringe contrast for  
 185  $\sim 1\%$  transmission through the liquid. Methanol, on the other hand, exhibits higher absorption  
 186 at 1550 nm, and thus the fringe contrast was beyond what the InGaAs camera could resolve.  
 187 In principle, a neutral density filter could be introduced in the reference arm to increase the  
 188 contrast; however, this was not needed to keep our uncertainties lower than the uncertainties in our  
 189 reference materials. We did not attempt this due to the added complexity. With acetonitrile, one  
 190 of the materials that exhibits high loss, we performed experiments at three different power levels  
 191 (25%, 50%, and 75% of max) at 1970 nm and did not observe any difference in the measured  
 192 index values that could arise from heating and thermal expansion, i.e., from the thermo-optic  
 193 effect [43].

194 Dispersion relations are obtained by fitting the Sellmeier equation:

$$n^2 - 1 = \frac{B_{UV}\lambda^2}{\lambda^2 - \lambda_{UV}^2} + \frac{B_{IR}\lambda^2}{\lambda^2 - \lambda_{IR}^2} \quad (2)$$

195 to the measured relative refractive index values. In Eq. 2,  $B_{UV}$  and  $B_{IR}$  are Sellmeier coefficients  
 196 and  $\lambda_{UV}$  and  $\lambda_{IR}$  are resonances in the UV and IR, respectively. Fits were obtained by using  
 197 Wolfram Mathematica’s “NonlinearModelFit” command with the Levenberg–Marquardt method.  
 198 The fitting algorithm automatically solved for  $B_{UV}$ ,  $B_{IR}$ , and  $\lambda_{UV}$  resonances, while  $\lambda_{IR}$   
 199 resonances were manually set to the strongest molecular vibration beyond 1970 nm obtained from  
 200 NIST [44] and AIST [45]. Although some of the liquids exhibit absorption bands in the SWIR

201 ( $\geq 1000$  nm), their refractive indices were fit using a single UV Sellmeier term (e.g., acetone).  
 202 On the other hand, for other liquids the inclusion of an IR term was necessary to enhance fitting  
 203 accuracy at longer wavelengths (e.g., most alcohols). Table 6 shows the Sellmeier coefficients  
 204 and resonances, in nanometers (nm), obtained by only fitting the data we measured. Note that we  
 205 extended these Sellmeier fits from 543.5 nm down to 400 nm with dotted lines for comparison  
 206 with literature experimental values; the uncertainty of results extrapolated down to 400 nm is  $\sim 5$   
 207 to 6 times greater than the uncertainty of the measured data. In Fig. 3 we compare our Sellmeier  
 208 fits and measured indices with data from Landolt–Börnstein [46] and from the broader literature  
 209 (see Tables 1–5 and the cited publications, excluding the starred values). We focus on literature  
 210 data at wavelengths from 400 nm to 2000 nm, and temperatures from 15 °C to 25 °C.

Table 6. Sellmeier coefficients for fits to the relative refractive index of different solvents. Wavelengths are expressed in nm, and the temperatures at which the data for these curves were measured are specified in Tables 1–5, ranging from 21.1 °C to 22.0 °C.

Solvent	$B_{UV}$	$\lambda_{UV}$	$B_{IR}$	$\lambda_{IR}$
Benzene	1.180	138	0	-
Toluene	1.171	134	0	-
p-Xylene	1.170	133	0	-
Pyridine	1.206	135	0	-
Nitrobenzene	1.302	159	0	-
Dichloromethane	0.9923	107	0	-
Chloroform	1.047	114	0	-
Carbon tetrachloride	1.094	99.6	0.290	12900
Methanol	0.7316	119	0	-
Ethanol	0.8312	96.4	0.0192	2970
1-Propanol	0.8940	94.4	0.0158	2970
1-Butanol	0.9314	95.9	0.0137	2970
1-Octanol	1.013	96.5	0.0112	2900
Carbon disulfide	1.502	169	0.163	6520
Pentafluorobenzonitrile	1.017	140	0	-
Bromotrichloromethane	1.211	120	0	-
Perfluorohexane	0.5532	90.0	0	-
Tetrachloroethylene	1.206	124	0	-
Trichloroacetoneitrile	1.030	103	0	-
Trifluoroacetic Anhydride	0.5939	99.7	0	-
Acetone	0.8144	108	0	-
Acetonitrile	0.7786	102	0	-
Hexane	0.8660	98.8	0	-
Cyclohexane	1.004	97.1	0.0108	3450
Tetrahydrofuran	0.9544	93.5	0.0147	3450
1,4-Dioxane	0.9937	98.2	0.0121	3450

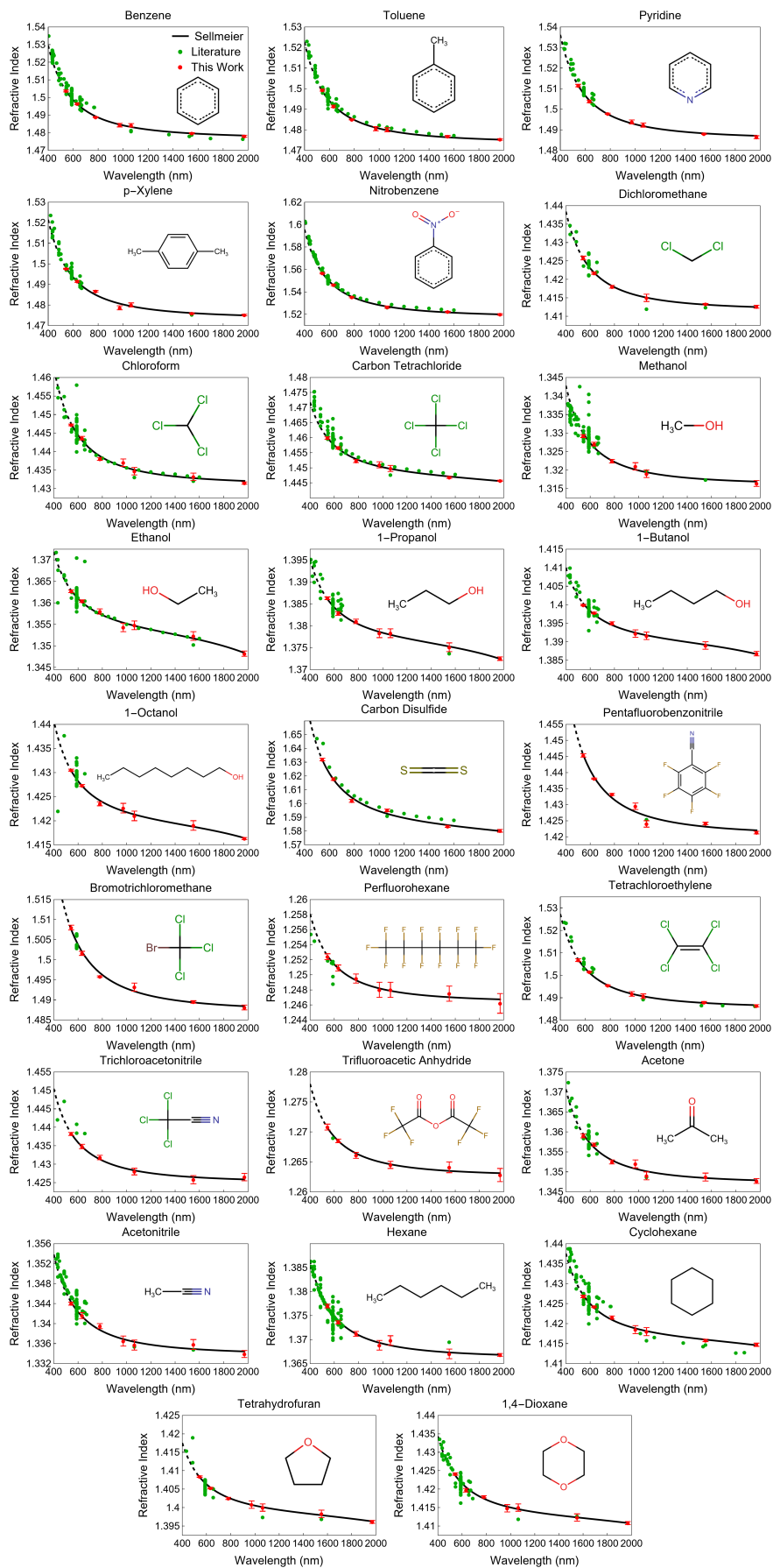


Fig. 3. Sellmeier fits of the relative refractive index data reported in this work and literature. Solid and dashed portions show fits to results measured in this work and their extrapolation, respectively. The temperatures associated with each solid curve are specified in Tables 1–5, ranging from 21.1 °C to 22.0 °C.

## 211 4. Conclusion

212 We developed a simple experimental technique to measure the refractive index of liquids relative  
213 known materials. This Rayleigh interferometer-based refractometer measures the refractive index  
214 by tracking the movement of the peaks of interference fringes the angle of incidence is varied. It  
215 is simple to set up, accurate (depending on the choice of reference material and curve fitting), and  
216 can effectively measure samples even in cases of relatively high absorption. This study presented  
217 the refractive index measurement of 26 solvents at 7 different wavelengths (543.5, 632.8, 780,  
218 973, 1064, 1550, and 1970 nm) and includes data from the literature. Thus, it extended the  
219 wavelength range deeper into the SWIR for most of these materials where data was not present.  
220 We also report the dispersion relationships for all the solvents using fitted Sellmeier equations to  
221 the above wavelengths extended to the range from 400 nm to 2  $\mu\text{m}$  juxtaposed with available  
222 reference data taken between 15 °C to 25 °C data.

223 **Funding.** Air Force Research Laboratory (AFRL) award, FA86511820019

224 **Acknowledgments.** We thank Scott Webster for fabricating the pinholes for producing the two beamlets,  
225 we thank Robert Norwood and Seth Marder for suggesting SWIR transparent liquids to characterize, and  
226 we thank Christian Keyser for introducing to us the lack of refractive index data in the IR, lending us the  
227 1970 nm thulium fiber laser laser, and for stimulating discussions. We also thank Markus Schmidt (private  
228 communication) for reports of a better fit to his liquid-filled fiber nonlinearities using our data for carbon  
229 tetrachloride.

230 **Disclosures.** The authors declare no conflicts of interest.

231 **Data availability.** Data underlying the results presented in this paper are available in Data File 1.

## 232 References

- 233 1. J. Campo, F. Desmet, W. Wenseleers, and E. Goovaerts, "Highly sensitive setup for tunable wavelength hyper-rayleigh  
234 scattering with parallel detection and calibration data for various solvents," *Opt. Express* **17**, 4587–4604 (2009).
- 235 2. S. Junaid, W. Huang, R. Scheibinger, K. Schaarschmidt, H. Schneidewind, P. Paradis, M. Bernier, R. Vallée, S.-E.  
236 Stanca, G. Zieger *et al.*, "Attenuation coefficients of selected organic and inorganic solvents in the mid-infrared  
237 spectral domain," *Opt. Mater. Express* **12**, 1754–1763 (2022).
- 238 3. F. M. Cox, A. Argyros, and M. C. J. Large, "Liquid-filled hollow core microstructured polymer optical fiber," *Opt.*  
239 *Express* **14**, 4135–4140 (2006).
- 240 4. Y. Zhu, X. Chen, Y. Xu, and Y. Xia, "Propagation properties of single-mode liquid-core optical fibers with  
241 subwavelength diameter," *J. Light. Technol.* **25**, 3051–3056 (2007).
- 242 5. R. Zhang, J. Teipel, X. Zhang, D. Nau, and H. Giessen, "Group velocity dispersion of tapered fibers immersed in  
243 different liquids," *Opt. Express* **12**, 1700–1707 (2004).
- 244 6. M. Vieweg, T. Gissibl, S. Pricking, B. T. Kuhlmeiy, D. C. Wu, B. J. Eggleton, and H. Giessen, "Ultrafast nonlinear  
245 optofluidics in selectively liquid-filled photonic crystal fibers," *Opt. Express* **18**, 25232–25240 (2010).
- 246 7. J. Bethge, A. Husakou, F. Mitschke, F. Noack, U. Griebner, G. Steinmeyer, and J. Herrmann, "Two-octave  
247 supercontinuum generation in a water-filled photonic crystal fiber," *Opt. Express* **18**, 6230–6240 (2010).
- 248 8. K. Kieu, L. Schneebeli, R. A. Norwood, and N. Peyghambarian, "Integrated liquid-core optical fibers for ultra-efficient  
249 nonlinear liquid photonics," *Opt. Express* **20**, 8148–8154 (2012).
- 250 9. M. Chemnitz, M. Gebhardt, C. Gaida, F. Stutzki, J. Kobelke, J. Limpert, A. Tünnermann, and M. A. Schmidt,  
251 "Hybrid soliton dynamics in liquid-core fibres," *Nat. Commun.* **8**, 42 (2017).
- 252 10. J. Liu, H. Schroeder, S. L. Chin, R. Li, and Z. Xu, "Nonlinear propagation of fs laser pulses in liquids and evolution  
253 of supercontinuum generation," *Opt. Express* **13**, 10248–10259 (2005).
- 254 11. L. Guyon, K. Hajek, F. Courvoisier, V. Boutou, R. Nuter, A. Vinçotte, S. Champeaux, L. Bergé, and J.-P. Wolf,  
255 "Control of lasing filament arrays in nonlinear liquid media," *Appl. Phys. B* **90**, 383–390 (2008).
- 256 12. D. P. Shelton, "Nonlocal hyper-rayleigh scattering from liquid nitrobenzene," *The J. Chem. Phys.* **132**, 154506 (2010).
- 257 13. D. Psaltis, S. R. Quake, and C. Yang, "Developing optofluidic technology through the fusion of microfluidics and  
258 optics," *Nature* **442**, 381–386 (2006).
- 259 14. C. Monat, P. Domachuk, and B. Eggleton, "Integrated optofluidics: A new river of light," *Nat. Photonics* **1**, 106–114  
260 (2007).
- 261 15. K. Kuhler, E. L. Dereniak, and M. Buchanan, "Measurement of the index of refraction of the plastic Phenoxy PKFE,"  
262 *Appl. Opt.* **30**, 1711–1714 (1991).
- 263 16. S. Kedenburg, M. Vieweg, T. Gissibl, and H. Giessen, "Linear refractive index and absorption measurements of  
264 nonlinear optical liquids in the visible and near-infrared spectral region," *Opt. Mater. Express* **2**, 1588–1611 (2012).

- 265 17. J. E. Saunders, C. Sanders, H. Chen, and H.-P. Loock, "Refractive indices of common solvents and solutions at 1550  
266 nm," *Appl. Opt.* **55**, 947–953 (2016).
- 267 18. B. Chandra and S. Bhaiya, "A simple, accurate alternative to the minimum deviation method of determining the  
268 refractive index of liquids," *Am. J. Phys.* **51**, 160–161 (1983).
- 269 19. D. Jenkins, "Refractive indices of solutions," *Phys. Educ.* **17**, 82 (1982).
- 270 20. A. Zaidi, Y. Makdisi, K. Bhatia, and I. Abutahun, "Accurate method for the determination of the refractive index of  
271 liquids using a laser," *Rev. Sci. Instruments* **60**, 803–805 (1989).
- 272 21. H. Hattori, H. Yamanaka, H. Kurniawan, S. Yokoi, and K. Kagawa, "Using minimum deviation of a secondary  
273 rainbow and its application to water analysis in a high-precision, refractive-index comparator for liquids," *Appl. Opt.*  
274 **36**, 5552–5556 (1997).
- 275 22. H. Hattori, H. Kakui, H. Kurniawan, and K. Kagawa, "Liquid refractometry by the rainbow method," *Appl. Opt.* **37**,  
276 4123–4129 (1998).
- 277 23. S. Nemoto, "Measurement of the refractive index of liquid using laser beam displacement," *Appl. Opt.* **31**, 6690–6694  
278 (1992).
- 279 24. F. Docchio, S. Corini, M. Perini, and R. Gasana, "A simple and reliable system for measuring the refractive index of  
280 liquids using a position-sensitive detector," *IEEE Trans. on Instrum. Meas.* **44**, 68–70 (1995).
- 281 25. D. P. Shelton, "Refractive index measured by laser beam displacement at  $\lambda = 1064$  nm for solvents and deuterated  
282 solvents," *Appl. Opt.* **50**, 4091–4098 (2011).
- 283 26. X. Wu, M. Muntzeck, T. de Los Arcos, G. Grundmeier, R. Wilhelm, and T. Wagner, "Determination of the refractive  
284 indices of ionic liquids by ellipsometry, and their application as immersion liquids," *Appl. Opt.* **57**, 9215–9222  
285 (2018).
- 286 27. X. Li, C. Wang, L. Ma, and L. Liu, "Ellipsometry-transmission measurement of the complex refractive indices for a  
287 series of organic solvents in the 200–1700 nm spectral range," *Infrared Phys. & Technol.* **125**, 104313 (2022).
- 288 28. T. L. Myers, R. G. Tonkyn, T. O. Danby, M. S. Taubman, B. E. Bernacki, J. C. Birnbaum, S. W. Sharpe, and T. J.  
289 Johnson, "Accurate measurement of the optical constants  $n$  and  $k$  for a series of 57 inorganic and organic liquids for  
290 optical modeling and detection," *Appl. Spectrosc.* **72**, 535–550 (2018).
- 291 29. C. Gouveia, M. Zibaii, H. Latifi, M. J. Marques, J. M. Baptista, and P. A. Jorge, "High resolution temperature  
292 independent refractive index measurement using differential white light interferometry," *Sensors Actuators B: Chem.*  
293 **188**, 1212–1217 (2013).
- 294 30. C. Sainz, J. Calatroni, and G. Tribillon, "Refractometry of liquid samples with spectrally resolved white light  
295 interferometry," *Meas. Sci. Technol.* **1**, 356 (1990).
- 296 31. A. Guerrero, C. Sainz, H. Perrin, R. Castell, and J. Calatroni, "Refractive index distribution measurements by means  
297 of spectrally-resolved white-light interferometry," *Opt. & Laser Technol.* **24**, 333–339 (1992).
- 298 32. S. Singh, "Refractive index measurement and its applications," *Phys. Scripta* **65**, 167 (2002).
- 299 33. H. El-Kashef, "The necessary requirements imposed on polar dielectric laser dye solvents," *Phys. B: Condens. Matter*  
300 **279**, 295–301 (2000).
- 301 34. H. El-Kashef, "Study of the refractive properties of laser dye solvents: toluene, carbon disulphide, chloroform, and  
302 benzene," *Opt. Mater.* **20**, 81–86 (2002).
- 303 35. S. De Nicola, P. Ferraro, A. Finizio, G. Pesce, and G. Pierattini, "Reflective grating interferometer for measuring the  
304 refractive index of transparent materials," *Opt. Commun.* **118**, 491–494 (1995).
- 305 36. P. Marteau, G. Montixi, J. Obriot, T. Bose, and J. St. Arnaud, "An accurate method for the refractive index  
306 measurements of liquids: Application of the kramers–krönig relation in the liquid phase," *Rev. Sci. Instruments* **62**,  
307 42–46 (1991).
- 308 37. P. Hariharan, *Optical Interferometry* (Academic Press, 1985).
- 309 38. K. Moutzouris, M. Papamichael, S. C. Betsis, I. Stavrakas, G. Hloupis, and D. Triantis, "Refractive, dispersive and  
310 thermo-optic properties of twelve organic solvents in the visible and near-infrared," *Appl. Phys. B* **116**, 617–622  
311 (2014).
- 312 39. A. Samoc, M. Samoc, B. Luther-Davies, R. Stockmann, H. Tillmann, and H.-H. Hoerhold, "Third-order optical  
313 nonlinearities of poly (arylamino-phenylenevinylene) studied with femtosecond pulses," in *Optoelectronics, Materials,*  
314 *and Devices for Communications*, vol. 4580 (SPIE, 2001), pp. 347–356.
- 315 40. I. Z. Kozma, P. Krok, and E. Riedle, "Direct measurement of the group-velocity mismatch and derivation of the  
316 refractive-index dispersion for a variety of solvents in the ultraviolet," *J. Opt. Soc. Am. B* **22**, 1479–1485 (2005).
- 317 41. J. E. Bertie, Z. Lan, R. N. Jones, and Y. Apelblat, "Infrared intensities of liquids XVIII: Accurate optical constants  
318 and molar absorption coefficients between 6500 and 800  $\text{cm}^{-1}$  of dichloromethane at 25° c, from spectra recorded in  
319 several laboratories," *Appl. spectroscopy* **49**, 840–851 (1995).
- 320 42. S. Ghosal, J. L. Ebert, and S. A. Self, "The infrared refractive indices of  $\text{CHBr}_3$ ,  $\text{CCl}_4$  and  $\text{CS}_2$ ," *Infrared Phys.* **34**,  
321 621–628 (1993).
- 322 43. J. N. Hayes, "Thermal blooming of laser beams in fluids," *Appl. Opt.* **11**, 455–461 (1972).
- 323 44. P. Linstorm, "Nist chemistry webbook, nist standard reference database number 69," *J. Phys. Chem. Ref. Data,*  
324 *Monogr.* **9**, 1–1951 (1998).
- 325 45. "AIST: Spectral database for organic compounds, SDBS," [https://sdb.sdb.aist.go.jp/sdb/s/cgi-bin/direct\\_frame\\_top.cgi](https://sdb.sdb.aist.go.jp/sdb/s/cgi-bin/direct_frame_top.cgi). Accessed: 2023-05-25.
- 326 46. C. Wohlfarth and M. Lechner, *Refractive Indices of Pure Liquids and Binary Liquid Mixtures (Supplement to III/38)*,

328  
329

Landolt-Börnstein: Numerical Data and Functional Relationships in Science and Technology - New Series (Springer Berlin Heidelberg, 2008).